

# Parameters of black holes in sources with periodic variability<sup>1</sup>

Oldřich SEMERÁK and Vladimír KARAS

*Faculty of Mathematics and Physics, Charles University Prague,  
V Holešovičkách 2, CZ-180 00 Praha 8, Czech Republic*

*E-mail: oldrich.semerak@mff.cuni.cz; vladimir.karas@mff.cuni.cz*

and

Fernando DE FELICE

*Department of Physics “G. Galilei”, University of Padova, Via Marzolo 8, I-35131 Padova, Italy*

*E-mail: defelice@padova.infn.it*

We discuss a way to deduce parameters of accreting black holes. The method employs properties of spectral features observed in radiation from an accretion disk. It is applicable to sources which exhibit periodic modulation of variability, provided: (i) Gravitational field is determined by the black hole and described by the Kerr metric; (ii) A thin accretion disk of a negligible mass lies in the equatorial plane of the hole; (iii) A secondary object (also with negligible mass) moves on a slightly inclined almost circular orbit around the black hole and passes periodically through the disk; (iv) The collisions result in observable photometric and spectroscopic features (temporal variability of the radiation flux and of spectral-line profiles produced in the disk), which show frequencies of orbital motion and of latitudinal oscillations; (v) One can measure width of the spectral line from hot spots arising in the disk due to collisions with the orbiter, and/or detect the predicted low-frequency oscillations, induced in the disk. These frequencies and the line width provide enough information to determine in physical units three parameters characterizing the source — the mass and angular momentum of the central black hole, and radius of the orbit of the secondary.

Keywords: Accretion disks — Black holes — X-rays: sources

---

<sup>1</sup>To appear in Publ. Astron. Soc. Japan (1999)

## 1. Introduction

There is an ever-growing theoretical and observational evidence that the dark masses present in some galactic nuclei and X-ray binaries are black holes (Rees 1998). Standard interpretation of observational data employs a black hole and an accretion disk or a torus (Kato et al. 1998). A number of ways have been suggested of how to deduce the properties of putative holes. The first rough estimates of their mass were based on energy considerations and limits implied by the shortest time-scales of variability. More precise methods became possible with modern observational techniques like HST, VLBI and X-ray satellites. Our present paper is relevant for sources with a rotating black hole surrounded by a thin accretion disk in the equatorial plane and a much less massive secondary orbiter passing periodically through the disk. First we briefly recall relevant spectral properties which have been discussed as possible observational signatures of a black hole (we do not mention other approaches which involve different physical mechanisms, e.g. gravitational waves).

In galactic nuclei, the existence and the size of the dark central mass are deduced from the profile of the surface brightness of the nuclei and from the spatial distribution and dynamics of surrounding gas and stars (Kormendy & Richstone 1995). Current optical and radio studies still probe only scales above  $10^4$  gravitational radii of the nucleus which is insufficient to resolve imprints of relativistic effects in the innermost regions around the centre, in particular to deduce the rate of its rotation. However, X-ray observations of the fluorescence iron  $K\alpha$  line (Nandra et al. 1997), especially its broad and variable profile skewed to lower energies, indicate that the Doppler and gravitational redshifts play a role and the emission takes place very near a rotating black hole. Several ways have been proposed to estimate parameters of the black holes in active galactic nuclei which rely on the source variability: for example, limits on the black-hole mass and its rate of rotation can be imposed from time delays between variations of the emission-line strength and of the continuum, and from temporal changes of the observed emission lines (e.g., Blandford & McKee 1982; Stella 1990; Bromley et al. 1997).

The evidence for stellar-mass black holes comes from observations of Galactic X-ray binaries where they are indicated by low luminosity of one of the

components, temporal variability, spectral features (mainly the presence of relatively strong ultrasoft component and of the hard X-ray tail), and the minimum mass of the dark component, as estimated from the mass function (e.g. Charles 1997). It has also been argued (Narayan et al. 1997) that the black-hole X-ray binaries could be distinguished by larger variation in luminosity between the bright and the faint states than is expected in the sources with neutron stars. This way of identifying black holes follows from the low radiative efficiency of advection-dominated accretion flows around black holes. Present observational evidence offers several objects of this type which show relatively stable periodic modulation (van der Klis 1997).

In the present contribution it is assumed that the disk remains in the equatorial plane and the modulating source is represented by a blob which keeps its identity for several orbital periods. A specific scheme for the signal modulation can be described in words as follows: The orbiter intersects the disk periodically and pulls gaseous material out its plane. This material temporarily obscures the disk, mainly at the radius of intersection, and affects radiation flux and emission-line profiles formed in that region and characterized by the observed widths. Phenomenologically, a spot forms in the disk and then it orbits around the center, surviving several orbital periods. Radiation of the spot modulates the observed radiation at the Keplerian frequency which is different from the frequency of collisions with the disk when the central black hole rotates. Both ingredients of the model, i.e. local physics of collisions with the disk and observed signal from orbiting spots, have been described in literature (recently, Ivanov et al. 1998; Karas 1997). In usual terminology the blob represents a hot spot, however, any perturbation of the disk surface emissivity (either bright, or less prominent due to obscuration) suffices for the purpose of phenomenological description.

Subsequent paragraphs describe technical details of the above-mentioned scenario. We will also show a predicted variable spectral feature involving relevant time-scales in a simplified situation.

## 2. Assumptions

Consider a system of a rotating black hole, an equatorial thin disk and a secondary orbiter (which may be a low-mass black hole — see Syer et al. 1991;

Vokrouhlický & Karas 1993). If both the disk and the secondary have negligible masses with respect to the central hole, the gravitational field is determined solely by the central black hole. In this situation, motion of the secondary is governed by Kerr metric, which in usual notation (Misner et al. 1973) acquires the form

$$ds^2 = -\Delta\Sigma\mathcal{A}^{-1}dt^2 + \Sigma\Delta^{-1}dr^2 + \Sigma d\theta^2 + \mathcal{A}\Sigma^{-1}\sin^2\theta(d\phi - \omega_K dt)^2; \quad (1)$$

here Boyer-Lindquist spheroidal coordinates  $(t, r, \theta, \phi)$  and geometrized units (in which  $c = G = 1$ ,  $c$  being the speed of light in vacuum and  $G$  the gravitational constant) have been used,  $M$  and  $a$  denote mass and specific rotational angular momentum of the centre,  $\Delta = r^2 - 2Mr + a^2$ ,  $\Sigma = r^2 + a^2 \cos^2 \theta$ ,  $\mathcal{A} = (r^2 + a^2)^2 - \Delta a^2 \sin^2 \theta$ , and  $\omega_K = 2Mar/\mathcal{A}$ .

World-line of the secondary is very close to a geodesic in the Kerr field, provided that the dynamical effect of passages through the disk is only weak, that tidal interaction is negligible (the secondary is assumed much smaller than the typical curvature radius of the field around), and that gravitational radiation is ignored. The trajectory undergoes three secular changes due to the interaction with the disk (Syer et al. 1991; Vokrouhlický & Karas 1993): long-term decrease of the semi-major axis (spiralling towards the centre due to energy dissipation in collisions with the disk), circularization (the orbit becomes spherical,  $r = \text{const}$ ), and gradual tilting of the orbit into the equatorial plane (the orbit declines to the disk). Since the time-scale for circularization is shorter than, or of the same order as, the time-scale necessary to drag the orbit into the disk, one can assume that the secondary follows a nearly equatorial spherical geodesic at late stages of evolution of the hole–disk–secondary system. The secondary remains on this type of orbit for a relatively long time. Let us note that we ignore gravity of the disk itself; the case of a massive disk was treated recently by Vokrouhlický & Karas (1998).

The resulting system is characterized by two angular frequencies — that of the azimuthal revolution of the orbiter around a Kerr black hole,  $\omega$ , and that of its latitudinal oscillations about the equatorial plane,  $\Omega_\infty$ . Both frequencies are in principle measurable at infinity provided that the passages of the orbiter produce strong enough modulation of the disk radiation (Karas & Vokrouhlický 1994 illustrated, by Fourier analysis of simulated photometric data, how these two peaks can be recognized in the power spectrum).

Relevant parameters of a quasi-circular orbit precessing with low amplitude about the equatorial plane of the Kerr spacetime are given in next section. Relations derived in Sect. 4. provide the parameters of the central black hole in terms of four observables — the three frequencies ( $\Omega_\infty$ ,  $\omega_+$ , and  $\kappa$ , as they are introduced in the text) and a spectral-line width. Equations can be solved easily if the secondary is not too close to the black hole (cf. the Appendix).

### 3. Parameters of the Precessing Orbit

For a general bound geodesic in the Kerr spacetime, the frequencies of the azimuthal and latitudinal motion can be given in terms of elliptic integrals (Karas & Vokrouhlický 1994). Relevant expressions acquire a simpler form in case of spherical geodesics (Wilkins 1972) and simplify still further for almost equatorial orbits. The azimuthal angular velocity  $\omega = d\phi/dt$  (with respect to a distant observer at rest) is then approximated by the Keplerian circular frequency

$$\omega_\pm = (a + 1/y_\pm)^{-1}, \quad (2)$$

where  $y_\pm = y(\omega_\pm) = \pm\sqrt{M/r^3}$  and the upper/lower sign corresponds to the prograde/retrograde orbit. We keep both cases for completeness, but only prograde trajectories (plus sign) will be considered later (the accretion disk is more likely to be corotating with the central black hole and the interaction with the disk makes also the secondary corotate eventually).

The proper angular frequency  $|\Omega|$  of small latitudinal harmonic oscillations about the equatorial plane is given, for a spherical orbit with steady radial component of acceleration, by (de Felice & Usseglio-Tomasset 1996; Semerák & de Felice 1997)

$$\Omega^2 = (u^t/r)^2 \{ \Delta\omega^2 + 2y_\pm^2 [a - (r^2 + a^2)\omega]^2 \}. \quad (3)$$

Here  $\omega = \text{const}$ , and the time component of four-velocity, given by  $(u^t)^{-2} = -g_{tt} - 2g_{t\phi}\omega - g_{\phi\phi}\omega^2$ , is approximated by the equatorial value

$$(u^t)^{-2} = 1 - (2M/r)(1 - a\omega)^2 - (r^2 + a^2)\omega^2. \quad (4)$$

Frequency of the collisions with the disk is twice the proper frequency  $|\Omega|$ ; the corresponding value measured by a distant observer is  $|\Omega_\infty| = |\Omega|/u^t$ . From eqs. (2)–(3), the explicit expression for a *free* orbit is

$$\begin{aligned} \Omega_\infty^2 &= \omega_\pm^2 (1 - 4ay_\pm + 3a^2/r^2) \\ &= \frac{\omega_\pm^2}{r^2} \left[ \Delta + 2(\sqrt{Mr} \mp a)^2 \right]. \end{aligned} \quad (5)$$

We remind that the frequency of latitudinal oscillations stands in the dispersion relation for corrugation waves in accretion disks. It has been suggested that  $\Omega_\infty$  could be detected in some QPO sources (Kato 1990).

The two eqs. (2) and (5) are not enough to fix the three unknowns  $M$ ,  $a$  and  $r$ . Another piece of information can be provided by the width of the emission line which is formed and modulated at the radius of successive collisions between the secondary and the disk. A stationary disk produces the well-known double-horn line profile which is more or less pronounced according to the inclination angle of the source. Radiation from each element in the disk experiences a frequency shift (Fanton et al. 1997)

$$g \equiv \frac{\nu_{\text{obs}}}{\nu_{\text{em}}} = u^t \frac{\omega_\pm}{y_\pm} \left[ 1 - \frac{2M}{r} + y_\pm (a + \sqrt{\Delta} e_{\hat{\phi}}) \right] \quad (6)$$

where  $e_{\hat{\phi}}$  is an emission direction cosinus (an azimuthal component of the unit vector along the direction of emission of a given photon, measured in the emitter's local frame), and

$$\begin{aligned} (u^t)^2 &= \frac{y_\pm^2}{\omega_\pm^2} \frac{1}{1 - 3M/r + 2ay_\pm} \\ &= \frac{M}{r} \frac{1}{\omega_\pm^2} \frac{1}{\Delta - (\sqrt{Mr} \mp a)^2} \end{aligned} \quad (7)$$

follows from (4) and (2). The observed total width of the line arises from the different frequency shifts  $g$  carried by photons which reach the observer at infinity. Since  $g$  depends on the emission cosinus  $e_{\hat{\phi}}$ , the maximum width of the line  $\delta g$  (which is a result of integration over one entire circle) corresponds to the range of  $e_{\hat{\phi}}$  consistent with the escape to infinity,  $\delta e_{\hat{\phi}}$ . We have from eq. (6)

$$(\delta g) = (\delta e_{\hat{\phi}}) u^t \omega_\pm \sqrt{\Delta}, \quad (8)$$

and thus

$$\begin{aligned} \delta^2 \equiv \frac{(\delta g)^2}{(\delta e_{\hat{\phi}})^2} &= \frac{M}{r} \frac{1 - 2M/r + a^2/r^2}{1 - 3M/r + 2ay_\pm} \\ &= \frac{M}{r} \frac{\Delta}{\Delta - (\sqrt{Mr} \mp a)^2}. \end{aligned} \quad (9)$$

From this equation it appears convenient to include the parameter  $\delta$  in our consideration because it can be written in the form independent of inclination angle. To determine  $\delta$  in terms of  $\delta g$ , one needs to fix

the range of  $\delta e_{\hat{\phi}}$ . This can be easily estimated for  $r \gg M$  (cf. Appendix). In general,  $\delta e_{\hat{\phi}}$  is at most 2 (which is acquired for  $\theta_o = \pi/2$ , i.e. edge-on view of the disk), and it decreases with the inclination angle  $\theta_o$  of the black hole–disk system relative to the line of sight (it also depends, quite weakly, on the rotational parameter  $a$  and the radius of emission  $r$ ). It appears unpractical to deal with a lengthy analytic expression for  $\delta e_{\hat{\phi}}$ . Instead, given  $a/M$ ,  $r/M$  and  $\theta_o$ , the actual value of  $\delta e_{\hat{\phi}}$  can be found by numerical ray tracing (Fanton et al. 1997).

We simulated a time-variable line profile to illustrate the main features expected in the observed signal (we used a modification of the code described by Karas and Vokrouhlický 1994). Figure 1 shows the measured count rate in the line (background subtracted) as a function of energy and orbital phase in the equatorial plane of an extreme ( $a = M$ ) Kerr black hole. In this example, only that contribution to the total light is taken into account which originates at  $10M \lesssim r \lesssim 14M$  where an orbiter affects the disk. Energy is normalized to the emission energy of the line in the local frame of the disk material, as usual (energy axis thus indicates the redshift factor  $g$ ). Phase axis is normalized with respect to Keplerian orbital motion at the central radius  $r = 12M$ , and interval of two periods is shown for clarity. One can observe:

(i) Modulation of the count rate in the line by the orbiter crossing the disk upwards at radius  $r$  with period  $T \equiv 2\pi/\Omega_\infty(r)$ . A flare is triggered at the moment of crossing and then falls off with time as the orbiting spot decays and the material swept out of the disk cools down (characteristic time-scale for this decay is taken to be two orbital periods; it is a phenomenological parameter here).

(ii) Another modulation by the orbiting spot with period  $t \equiv 2\pi/\omega_+$ . Corresponding maxima of the count rate can be seen at phase equal to 0.5, 1.5, ... (due to Doppler boosting).

(iii) Orbital variation  $\delta g$  of the redshift factor (also with periodicity  $t$ ) in projection down into the energy-phase plane.

In Fig. 1 inclination angle has been taken 40 deg. Obviously, any non-zero inclination would lead to a qualitatively similar picture. However, at higher inclinations ( $\gtrsim 60$  deg) another local maximum would develop in the observed flux due to the lensing effect. (Its position is advancing in phase by  $\approx 0.25$  with

respect to the Doppler peak.) Difference in the two frequencies,  $\Omega_\infty$  and  $\omega_+$ , discussed in previous paragraphs translates to the time gap  $T - t$ . Let us emphasize that this figure offers a qualitative illustration of the predicted time-variable spectral feature. In a more realistic model one needs to take into account a proper method of background continuum subtraction (underlying continuum has been ignored here). Mutual interplay between spectral features (around 6.4 keV) and continuum has been subject of recent works (Young et al. 1998; Życki et al. 1998; Martocchia et al. 1999) which show substantial smoothing of the profile in some situations.

Uncertainties connected with the badly known  $\delta e_{\hat{\phi}}$  can be overcome by introducing another independent observable. A promising possibility arises from a more realistic view of the star-disk collision. As mentioned above, the collisions disturb the disk periodically with latitudinal frequency (5). If the orbiter passes across the disk at small  $r$ , it may induce waves in the disk matter which remain trapped in the range of several gravitational radii and are governed by epicyclic frequency  $\kappa$  (Okazaki et al. 1987; Nowak & Wagoner 1992):

$$\begin{aligned}\kappa^2 &= \omega_\pm^2 (1 - 6M/r + 8ay_\pm - 3a^2/r^2) \\ &= \frac{\omega_\pm^2}{r^2} [\Delta - 4(\sqrt{Mr} \mp a)^2].\end{aligned}\quad (10)$$

These modes can be excited and trapped in a rather narrow range of radius, and one can thus expect that they will reflect just the orbital radius of the satellite. However, the problem of distinguishing between different possible modes is a subject of much debate and has not yet been settled.

#### 4. Determining $M$ , $a$ , and $r$

The formulas (2), (5), (9) and/or (10) provide a closed system of ordinary equations for  $M$ ,  $a$  and  $r$  (and possibly  $\delta e_{\hat{\phi}}$ , if one succeeds in measuring all four observables) as functions of the quantities  $\omega_\pm$ ,  $|\Omega_\infty|$ ,  $|\delta|$  and/or  $|\kappa|$ . The equations can be tackled in different manners depending on which of the quantities is determined with the best confidence. Now we discuss derivation of the most desired combinations of parameters,  $r/M$  and  $a/M$ , from different starting relations:

(i) With the knowledge of  $|\Omega_\infty|$  and  $|\kappa|$  one can start

from eqs. (5) and (10) and find

$$\frac{\Delta}{r^2} = \frac{2\Omega_\infty^2 + \kappa^2}{3\omega_\pm^2}, \quad (11)$$

$$\frac{(\sqrt{Mr} \mp a)^2}{r^2} = \frac{\Omega_\infty^2 - \kappa^2}{6\omega_\pm^2}, \quad (12)$$

which can be solved with respect to  $M/r$  and  $a/r$ :

$$\begin{aligned}\frac{M}{r} &= 1 - \frac{\Omega_\infty^2 + 5\kappa^2}{6\omega_\pm^2} - 2 \left( \frac{\Omega_\infty^2 - \kappa^2}{6\omega_\pm^2} \right)^{1/2} \\ &\quad \times \left( 1 - \frac{\Omega_\infty^2 + 2\kappa^2}{3\omega_\pm^2} \right)^{1/2},\end{aligned}\quad (13)$$

$$\frac{a^2}{r^2} = \frac{2\Omega_\infty^2 + \kappa^2}{3\omega_\pm^2} + \frac{2M}{r} - 1. \quad (14)$$

The values of  $r/M$  and  $a/M$  are reached then by obvious manipulations. One more relation is needed to obtain the absolute values  $M$ ,  $a$  and  $r$ . Using eq. (2), we fix

$$\frac{1}{r} = \left( \frac{a}{r} \pm \sqrt{\frac{r}{M}} \right) \omega_\pm; \quad (15)$$

$M$  and  $a$  follow from above.

(ii) Starting from eq. (9), a convenient possibility is to combine it with eqs. (5) and (10). We find

$$\delta^2 = \frac{2M}{3r} \frac{2\Omega_\infty^2 + \kappa^2}{\Omega_\infty^2 + \kappa^2}, \quad (16)$$

and thus the value of  $M/r$  follows immediately. This can be compared with the result (13) to fix (or verify) the value of  $\delta e_{\hat{\phi}}$ .

(iii) Suppose we know  $\omega_\pm$ ,  $|\Omega_\infty|$  and  $|\delta|$ . Introducing

$$a = \omega_\pm^{-1} - y_\pm^{-1} \quad (17)$$

from eq. (2) to eqs. (5) and (9), we obtain

$$r^2 = \frac{3(1 - \omega_\pm/y_\pm)^2}{4\omega_\pm y_\pm + \Omega_\infty^2 - 5\omega_\pm^2}; \quad (18)$$

$y_\pm$  is then given by quartic equation. This is rather cumbersome to be handled analytically and it is more suitable to find the solution numerically for each given set of data. However, a simple explicit solution can be found analytically if  $r^2 \gg a^2$ ; see the Appendix.

(iv) The case when one measures  $\omega_\pm$ ,  $|\kappa|$  and  $|\delta|$ , and thus turns to eqs. (2), (10) and (9), also leads to a quartic equation.

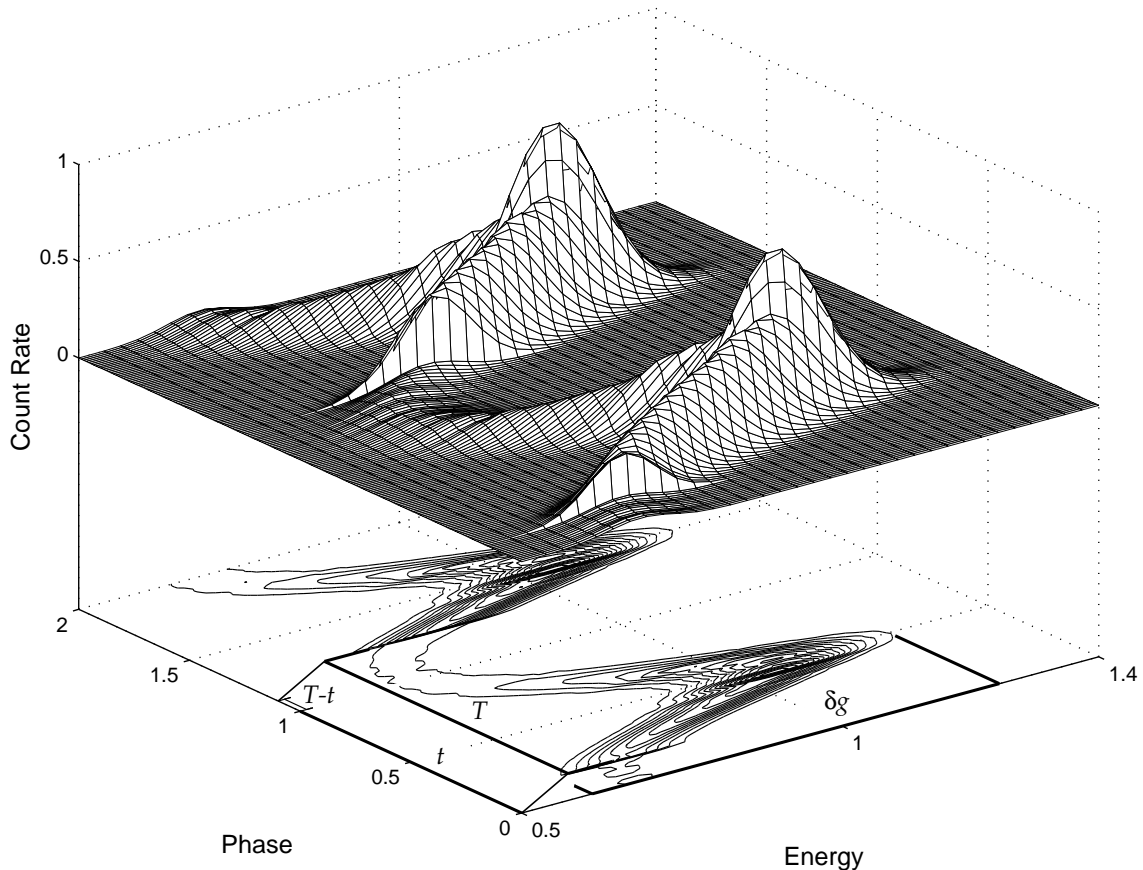


Fig. 1. Simulation of the time-variable line profile from a hot spot orbiting with the disk. A flare occurs at the moment of the star-disk collision (the sharp increase in flux), giving rise to a spot on the disc surface. Observed count rate is then modified by orbital motion of the spot (period  $t$ ) and by relativistic lensing (with a corresponding change of energy in the range  $\delta g$ ). The spot decays gently with time, until another one is generated in a subsequent collision (i.e. after period  $T$ ). This graph has been obtained by ray tracing in the Kerr metric. Decay time of the spot is taken as a free parameter. See the text for details.

In the Schwarzschild case,  $a = 0$ , eqs. (2) and (5) are reduced to

$$\omega_{\pm} = y_{\pm} = \pm |\Omega_{\infty}| = \pm \sqrt{M/r^3}, \quad (19)$$

eq. (9) reads

$$\delta^2 = r^2 \omega_{\pm}^2 \frac{1 - 2r^2 \omega_{\pm}^2}{1 - 3r^2 \omega_{\pm}^2} \quad (20)$$

and eq. (10)

$$\kappa^2 = \omega_{\pm}^2 (1 - 6M/r). \quad (21)$$

The physical solution of eq. (20) is

$$r^2 = (4\omega_{\pm}^2)^{-1} \left[ 3\delta^2 + 1 - \sqrt{(3\delta^2 + 1)^2 - 8\delta^2} \right] \quad (22)$$

while that of eq. (21)

$$r^2 = (6\omega_{\pm}^2)^{-1} (1 - \kappa^2/\omega_{\pm}^2); \quad (23)$$

$M$  follows then from eq. (19).

Note that the above formulas are written in geometrized units. Corresponding quantities in physical

units are obtained by the following conversions:

$$\frac{M^{\text{phys}}}{M_{\odot}^{\text{phys}}} = \frac{M}{1.477 \times 10^5 \text{cm}}, \quad (24)$$

$$a^{\text{phys}} = ca, \quad r^{\text{phys}} = r; \quad (25)$$

also

$$\frac{a}{M} = \frac{a^{\text{phys}}}{GM^{\text{phys}}/c}, \quad \frac{r}{M} = \frac{r^{\text{phys}}}{GM^{\text{phys}}/c^2}. \quad (26)$$

To obtain frequency in physical units [Hz] (either from  $\omega$  or  $\Omega$ ), one uses the relation

$$f^{\text{phys}} = \frac{\omega^{\text{phys}}}{2\pi} = \frac{c\omega}{2\pi} = (4.77 \times 10^9 \text{cm/s})\omega. \quad (27)$$

In usual notation of relativistic astrophysics the (geometrized) frequencies are scaled by  $M^{-1}$  (as in Tab. 1). Their numerical values must be multiplied by factor

$$\frac{c}{2\pi M} = (3.231 \times 10^4) \left(\frac{M}{M_{\odot}}\right)^{-1} \text{ [Hz]}. \quad (28)$$

## 5. Discussion

We examined an interesting possibility of determining the intrinsic parameters of a black hole – accretion disk system in sources with periodic modulation of variability which is caused by an orbiting satellite. The method combines different pieces of information contained in time-variable spectral and photometric signal, which have been discussed (widely but separately) in the recent literature. It can provide all the relevant quantities in physical units, but of course it can also be combined with another independent determination of some of the parameters. We assumed that the orbiting secondary is only weakly affected by the disk, which allowed us to approximate its orbit by a nearly equatorial spherical geodesic. This restriction must be abandoned if the secondary is not compact enough.

The proposed approach can be applied to galactic nuclei as well as to stellar-mass objects in the Galaxy, but identity and physical properties of the secondary depend on the mass of the centre around which it revolves. In the latter case the lifetime of the system is more restricted by tidal interactions and the secondary appears unlikely to survive long enough. Effects of tidal distortion of a stellar body passing near a black hole have been discussed by several authors who show that the star becomes squeezed and

heated (Rees 1988; Luminet & Marck 1985; Evans & Kochanek 1989). Tidal disruption occurs in case of a close encounter, when the satellite plunges below the tidal radius  $R_t \sim 10^{11} (M/M_*)^{1/3} (R_*/R_{\odot})$  cm, where  $M_*$  and  $R_*$  denote the mass and the radius of the satellite. On the other hand, distortions of a compact satellite near a supermassive black hole are negligible. Duration of a spot or a vortex in an accretion disk has been also discussed by several authors but remains still uncertain (Adams & Watkins 1995; Bracco et al. 1998). We assumed that the lifetime exceeds the corresponding orbital period.

Several possible targets have been discussed already. For example, optical outbursts in the blazar OJ 287 have recently been modelled in terms of a black-hole binary system by Villata et al. (1998). The source exhibits several time-scales: feature-less short-term variability, 12-yr cycle, and, possibly, a 60-yr cycle. These authors, however, presume both components to be of comparable masses while in our calculation frequencies are determined under the assumption that the secondary is much less massive than the primary (cf. also Sundelius et al. 1997). There are more BL Lac objects which show a periodic component of optical variability but time-scales are always  $\gtrsim 10$  yrs in the optical band, and statistical compilation of data is therefore very difficult (Liu et al. 1997). As a better example, a 16-hr periodicity was reported in the X-ray signal from the Seyfert galaxy IRAS 18325-5926 (Iwasawa et al. 1998).

We conclude with M. J. Rees (1998): *There is a real chance that someday observers will find evidence that an AGN is being modulated by an orbiting star, which would act as a test particle whose orbital precession would probe the metric in the domain where the distinctive features of the Kerr geometry should show up clearly.* Indeed, to be able to resolve the effects of general relativity in AGN, the satellite would have to orbit near the centre and produce periodicity on a few-hours time-scale.

O. S. thanks the University of Padova and the International Centre for Theoretical Physics in Trieste for hospitality, and he acknowledges support from the grant GACR 202/99/0261 in Prague. F. de F. thanks for support from Agenzia Spaziale Italiana, Gruppo Nazionale per la Fisica Matematica del C.N.R., and Ministero della Ricerca Scientifica e Tecnologica of Italy. V. K. thanks for hospitality of the International School for Advanced Studies in Trieste; support from

Table 1. Accuracy of approximative relations (30)–(31).

Here,  $a$  and  $r$  stand as input parameters of the system (black-hole angular momentum and radius of the orbit of the secondary, respectively). Corresponding values of  $\tilde{a}$  and  $\tilde{r}$  are deduced from our approximative equations as given in the Appendix.

$a$	$r$	$\omega_+$	$\Omega_\infty$	$\delta$	$\tilde{a}$	$\tilde{r}$
0.30	5	0.08711	0.08279	0.5158	0.335	5.4
	10	0.03133	0.03077	0.3338	0.311	10.2
	20	0.01114	0.01107	0.2292	0.303	20.1
	40	0.00395	0.00394	0.1600	0.301	40.1
0.60	5	0.08489	0.07727	0.4921	0.762	5.7
	10	0.03103	0.03001	0.3300	0.644	10.4
	20	0.01111	0.01097	0.2284	0.614	20.3
	40	0.00394	0.00393	0.1598	0.605	40.2
0.85	5	0.08312	0.07353	0.4773	1.305	5.9
	10	0.03080	0.02944	0.3273	0.943	10.6
	20	0.01108	0.01089	0.2278	0.878	20.4
	40	0.00394	0.00392	0.1597	0.859	40.3
1.00	5	0.08210	0.07168	0.4702	1.636	6.0
	10	0.03065	0.02914	0.3258	1.135	10.7
	20	0.01106	0.01085	0.2274	1.039	20.4
	40	0.00394	0.00391	0.1596	1.013	40.3

the grants GACR 205/97/1165 and 202/98/0522 is acknowledged.

## 6. Appendix. A Simple Explicit Solution of Eqs. (2), (5) and (9) for $r^2 \gg a^2$

It is relevant to suppose that the secondary orbits at  $r \gtrsim 10M$ , and typically at  $r \sim 30M$ . In this region a significant part of the disk radiation arises. Also, the secondary would be tidally disrupted if it plunges too close to the black hole horizon (to  $r \sim M$ ), while at too large orbital radius the relativistic dragging effect vanishes (with  $\propto r^{-3}$ ) and the frequencies  $\omega_\pm$ ,  $|\Omega_\infty|$  would become indistinguishable.

At large enough radii ( $r \sim 30M$ ), several terms in eqs. (2), (5) and (9) become negligible when compared with the rest. Ignoring them, one arrives at a simplified set of relations which keeps an acceptable precision of the resulting parameters without the need to solve the fourth-order equation. (Exact equations can be used to improve the estimates numerically.) One chooses some particular approximation according to what precision is desired at each of the quantities  $M$ ,  $a$ ,  $r$ , and also according to precision of each of the input data  $|\omega_\pm|$ ,  $|\Omega_\infty|$ ,  $|\delta|$ . For instance, since

$ay_\pm < 1/30$ , we can take

$$\omega_\pm \simeq y_\pm(1 - ay_\pm), \quad y_\pm \simeq \omega_\pm(1 + a\omega_\pm)$$

(for the determination of  $M$  from the known  $r$ , or vice versa, it is even sufficient to neglect  $ay_\pm$  altogether and use just the Schwarzschild form of equations). Other two relevant bounds are:

$$\frac{a^2/r^2}{2M/r} < \frac{1}{20}, \quad \frac{a^2/r^2}{ay_\pm} = \frac{ay_\pm}{M/r} = \frac{a}{\sqrt{Mr}} < \frac{1}{3}.$$

An example of a reasonable estimate is provided as follows (we suppose a prograde orbit of the secondary, and consequently we take plus sign in the relations): Restricting to the Schwarzschild limit of eq. (9),

$$\delta^2 = \frac{M}{r} \frac{1 - 2M/r}{1 - 3M/r}, \quad (29)$$

one comes to an approximative value for  $M/r$  (the approximative values will be denoted by a tilde below),

$$4\tilde{M}/\tilde{r} = 1 + 3\delta^2 - \sqrt{(1 + 3\delta^2)^2 - 8\delta^2}. \quad (30)$$

Approximative expression for  $a/r$  follows then from eq. (5):

$$\frac{3\tilde{a}}{\tilde{r}} = 2\sqrt{\frac{\tilde{M}}{\tilde{r}}} - \sqrt{4\frac{\tilde{M}}{\tilde{r}} - 3\left(1 - \frac{\Omega_\infty^2}{\omega_+^2}\right)}. \quad (31)$$

Finally, eq. (2) yields  $1/\tilde{r}$  according to the relation (15). The unknowns  $\tilde{M}$ ,  $\tilde{a}/\tilde{M}$  and  $\tilde{r}/\tilde{M}$  are reached by obvious combinations.

The results of this approximation are illustrated in Table 1 for several typical  $a$  and  $r$ , together with the respective values of the observable quantities. Here,  $a$  and  $r$  are assumed to be given (in units of  $M$ ; see the text above for conversions to physical units). For a prograde orbit of the secondary,  $\omega_+$  and  $\Omega_\infty(\omega_+)$  are the corresponding azimuthal and latitudinal angular frequencies,  $\delta = \delta(\omega_+)$  is the dimensionless parameter defined by eq. (9). From these quantities one computes the estimates  $\tilde{a}$  and  $\tilde{r}$  (in units of  $\tilde{M}$ ) using our approximate eqs. (30)–(31). Notice that acceptable results are reached for  $r \gtrsim 10M$  where approximative values are close to the simulated exact ones. Accuracy decreases if the secondary orbits too close. On the other hand, too distant orbits are also unsuitable: dragging effects weaken quickly with distance



from the centre and the values of  $\omega_+$  and  $\Omega_\infty$  become too close to each other. In other words, the minimum sampling rate (inverse of the Nyquist critical frequency; Press et al. 1992) is restricted by the difference  $\tau = \Omega_\infty^{-1} - \omega_+^{-1}$ , requiring that both frequencies can be safely distinguished in the observed signal. For example, for  $M = 10^8 M_\odot$ , maximum rotation ( $a = 1$ ), and  $r = 20$  gravitational radii, one can find (from Table 1)  $\tau = 1.8$ , which in Fig. 1 corresponds to time interval  $T - t = 2\pi M c^{-1} \tau = 1.5$  hr.

## References

- Adams, F. C., Watkins, R. 1995, ApJ 451, 314
- Blandford, R. D., McKee, C. F. 1982, ApJ 255, 419
- Bracco, A., Provenzale, A., Spiegel, E. A., Yecko, P. 1998, in Theory of Black Hole Accretion Disks, eds. M. A. Abramowicz, G. Björnson, J. E. Pringle (Cambridge University Press, Cambridge)
- Bromley, B. C., Chen, K., Miller, W. A. 1997, ApJ 475, 57
- Charles, P. A. 1997, in Proc. 18th Texas Conference (World Scientific, Singapore), in press
- de Felice, F., Usseglio-Tomasset, S. 1996, Gen. Rel. Grav. 28, 179
- Evans, C. R., Kochanek, C. S. 1989, ApJ 346, L13
- Fanton, C., Calvani, M., de Felice, F., Čadež, A. 1997, PASJ 49, 159
- Ivanov, P. B., Igumenshchev I. V., Novikov I. D. 1998, ApJ 507, 131
- Iwasawa, K., Fabian, A. C., Brandt, W. N., Kunieda, H., Misaki, K., Reynolds, C. S., Terashima, Y. 1998, MNRAS 295, L20
- Karas, V. 1997, MNRAS 288, 12
- Karas, V., Vokrouhlický, D. 1994, ApJ 422, 218
- Kato, S. 1990, PASJ 42, 99
- Kato, S., Fukue, J., Mineshige, S. 1998, Black-hole Accretion Disks (Kyoto University Press, Kyoto)
- Kormendy, J., Richstone, D. 1995, ARAA 33, 581
- Liu, F. K., Liu, B. F., Xie, G. Z. 1997, AAS 123, 569
- Luminet, J.-P., Marck, J.-A. 1985, MNRAS 212, 57
- Martocchia, A., Karas, V., Matt, G. 1999, MNRAS, submitted
- Misner, C. W., Thorne, K. S., Wheeler, J. A. 1973, Gravitation (Freeman, San Francisco)
- Nandra, K., George, I. M., Mushotzky, R. F., Turner, T. J., Yaqoob, T. 1997, ApJ 476, 70; ApJ 477, 602
- Narayan, R., Garcia, M. R., McClintock, J. E. 1997, ApJ 478, L79
- Nowak M. A., Wagoner R. V. 1992, ApJ 393, 697
- Okazaki, A. T., Kato, S., Fukue, J. 1987, PASJ 42, 99
- Press, W. H., Teukolsky, S. A., Vetterling, W. T., Flannery, B. P. 1992, Numerical Recipes (Cambridge University Press, Cambridge)
- Rees, M. J. 1988, Nature 333, 523
- Rees, M. J. 1998, in Black Holes and Relativistic Stars, ed. R. M. Wald (Univ. Chicago Press, Chicago)
- Semerák, O., de Felice, F. 1997, Class. Quantum Grav. 14, 2381
- Stella, L. 1990, Nature 344, 747
- Sundelius, B., Wahde, M., Lehto, H. J., Valtonen, M. J. 1997, ApJ 484, 180
- Syer, D., Clarke, C. J., Rees, M. J. 1991, MNRAS 250, 505
- Young A. J., Ross R. R., Fabian A. C. 1998, MNRAS 300, L11
- van der Klis, M. 1997, in Proc. NATO ASI, The Many Faces of Neutron Stars; astro-ph/9710016
- Villata, M., Raiteri, C. M., Sillanpää, A., Takalo, L. O. 1998, MNRAS 293, L13
- Vokrouhlický, D., Karas, V. 1993, MNRAS 265, 365
- Vokrouhlický, D., Karas, V. 1998, MNRAS 298, 53
- Wilkins, D. C. 1972, Phys. Rev. D 5, 814
- Życki P. T., Done C., Smith D. A. 1998, ApJ 496, L25

# Twin peaks separation in sources with kHz QPOs caused by orbital motion<sup>2</sup>

Vladimír Karas<sup>1</sup>

The expected range of kilohertz quasi-periodic oscillations (kHz QPOs) is studied regarding low-mass X-ray binaries with twin peaks in their Fourier spectra. The twin peaks are interpreted as combination of epicyclic and precession frequencies in Schwarzschild metric. If the pairs are caused by general relativistic orbital motion of gaseous clumps around a neutron star, then moderate size of the clumps and eccentricity of their orbits can account for the non-constant peaks separation reported in Scorpius X-1 and 4U 1608-52. The neutron stars mass comes out in the range 1.6–1.9 solar masses. Variation in the orbital parameters of the clumps translates into an expected range in the plot of pair separation versus frequency, typically showing a decreasing slope.

Keywords: X-rays: stars — stars: individual (Sco X-1, 4U 1608-52) — relativity

---

<sup>2</sup>To appear in The Astrophysical Journal (1999)

<sup>1</sup>Astronomical Institute, Charles University Prague, V Holešovičkách 2, CZ-180 00 Praha 8, Czech Republic; vladimir.karas@mff.cuni.cz

## 7. Introduction

Accreting low-magnetic field neutron stars exhibit complex behaviour including X-ray variability on millisecond time-scales; see van der Klis (1998) for a review of millisecond phenomena in low-mass X-ray binaries, and its recent update (van der Klis 1999). Cf. Méndez (1999) for a recent summary of *RXTE* observational results and for further references. Here we concentrate on the widely discussed twin kHz peaks which so far have been reported in the Fourier power spectra of nearly twenty objects. The importance of this feature follows from the fact that the positions of the two peaks (and of the third, burst oscillation frequency), their large coherence and variation with the count rate restrict viable models of the accreting body and of the geometry of the system. Also, it turns out that effects of general relativity cannot be ignored (Kluźniak 1998; Stella & Vietri 1998; Zhang et al. 1998).

The approximately constant separation of the twin QPO peaks indicates that some kind of beat-frequency relation (Miller, Lamb, & Psaltis 1998) can explain these pairs, although the simplest models have been challenged by the discovery of QPO sources in which the separation of the peaks decreases as their frequency increases: Sco X-1 (van der Klis et al. 1997) and 4U 1608-52 (Méndez et al. 1998). Other sources are consistent with this trend too, e.g., 4U 1735-44 (Ford et al. 1998) and 4U 1728-34 (Méndez & van der Klis 1999). An inspiring alternative has recently been proposed by Stella & Vietri (1999) who introduce frequencies of the orbital motion around a compact body, namely orbital frequency, epicyclic frequency, and their difference. Here, this idea will be further studied. In particular, the range of expected frequency variation of the twin peaks will be estimated assuming that the feature arises from the motion of clumps with small but finite size, orbiting along eccentric orbits. The aim is to examine the main difference of this interpretation against simple constant-separation scenario by quantifying the expected separation as a function of peaks frequency. The mass of the neutron star stands as a parameter of the procedure in which predicted frequencies are fitted to data. It will be shown that the picture is indeed in agreement with the decreasing difference of the QPO peaks in Sco X-1 and 4U 1608-52. Even more importantly, the model is testable in principle, and it can be rejected when predicted frequencies of the peaks are found inconsistent with more accurate data in future.

## 8. Frequencies relevant for the twin peaks

Gravitational field is described in terms of Schwarzschild metric (specified by the mass  $M$  of the body which is taken to be of the order of two solar masses). We will first write down expressions for the two fundamental frequencies driving the orbital motion of blobs, which are

assumed to follow free trajectories (Chandrasekhar 1983). This is the simplest situation which of course will have to be abandoned in a more realistic model when the influence of radiation and of magnetic forces is taken into account, or when the gravitational field itself contains higher multipoles. Trajectories in a spherical gravitational field of Schwarzschild metric are planar but, in general, they do not form a closed curve in space. In the case of bound stable orbits satisfying the condition

$$1 - 6\mu - 2\mu e \geq 0, \quad \mu \equiv Ma^{-1} (1 - e^2)^{-1}, \quad (1)$$

one can associate eccentricity  $e$  and semimajor axis  $a$  with corresponding values of pericentre ( $r_p$ ) and apocentre ( $r_a$ ) distances,  $e = (r_a - r_p)/(r_a + r_p)$ ,  $a = r_p/(1 - e)$ . The orbit can be characterized by the pericenter shift  $\delta\phi_p$  during period  $P$  of time which elapses between subsequent passages through pericentre of the orbit. (Here, temporal quantities are expressed with respect to a distant observer at rest and measured in geometrized units, while azimuthal angles are defined in the orbital plane in the standard manner). Both  $\delta\phi_p$  and  $P$  can be written in the form of integrals over relativistic true anomaly  $\bar{\chi}$ ,

$$\delta\phi_p = \int_0^{2\pi} [1 - 2\mu(3 + \eta)]^{-1/2} d\bar{\chi} - 2\pi, \quad (2)$$

$$P = \mathcal{M} \int_0^{2\pi} (1 + \eta)^{-2} [1 - 2\mu(3 + \eta)]^{-1/2} \times [1 - 2\mu(1 + \eta)]^{-1} d\bar{\chi}, \quad (3)$$

where  $\eta = e \cos \bar{\chi}$ ,  $\mathcal{M} = M\mu^{-3/2} \sqrt{(2\mu - 1) - (2\mu e)^2}$ . The frequency of radial oscillations (epicyclic frequency) is thus  $\nu_r = P^{-1}$ , and precession frequency  $\nu_p = \delta\phi_p/(2\pi P)$ . Combination of these two frequencies gives the corresponding azimuthal frequency,  $\nu_\phi - \nu_p = \nu_r$ .<sup>3</sup> Eqs. (2)–(3) can be written in terms of elliptic integrals (Karas & Vokrouhlický 1994). Frequencies are then given in a more elegant form, although direct numerical evaluation of integrals (2)–(3) is equivalent for practical purposes.

Several instability mechanisms have been identified which may set clumps of gaseous material onto an eccentric orbit down from the inner edge of an accretion disk

<sup>3</sup>These quantities are introduced in standard manner, similar to Stella & Vietri (1999). Notice, however, that our definition of  $\nu_p$  differs slightly from their corresponding relation for  $\nu_{per}$ , because here it is expressed in terms of the integral over the *whole range* of  $2\pi$  in true anomaly. This is a proper and natural definition although the difference is only moderate for low-eccentricity orbits, considered in these papers. For eccentric orbits around  $6M$ , azimuthal and precession frequencies are comparable while frequency of radial oscillations is much less.

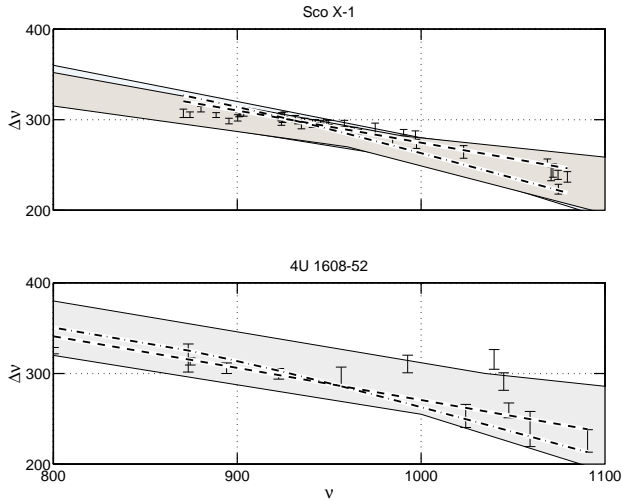


Fig. 1.— The best fits in the plot of the pair separation  $\Delta\nu(\nu)$  for  $\nu = \nu_\phi$  (dot-dashed) and  $\nu = \nu_p$  (dashed), respectively. For the latter case, shaded regions indicate the expected variation  $\Delta\nu$  as function of the upper peak frequency  $\nu$ . Notice that interpretation of peaks in terms of epicyclic and precession frequencies with reasonable variation of free parameters covers the data and captures the trend of decreasing  $\Delta\nu(\nu)$ . Frequencies are in Hertz. See the text for further details.

or from the sonic point. Miller et al. (1998) remark that there may even be hundreds of clumps accumulated near the sonic point which can subsequently be set on an inspiralling trajectory. There is an interesting possibility which concerns freely moving clumps: a *steady eccentric ring* may be formed from individual blobs, surviving a number of orbital periods and rotating with precession frequency  $\nu_p$  (Bao, Hadrava, & Østgaard 1994). This presumes that clumps of matter are set on the eccentric orbit ( $a, e$  given) near the apocentre, one after another. Radiation from illuminated or self-radiating clumps is modulated at orbital and precession frequencies, and their differences also appear in the harmonic content of the observed signal. We thus examined the possibility of interpreting the difference between the two peaks as  $\Delta\nu = \nu_r$ , while the upper twin peak can be interpreted either as  $\nu = \nu_\phi$  (as in Stella & Vietri 1999), or alternatively as  $\nu = \nu_p$ . As we show later on, both interpretations lead to acceptable agreement with data on the peak frequencies in Sco X-1 and 4U 1608-52, but the latter one corresponds to the masses of the neutron star which are lower by about  $0.3M_\odot$ .

The frequencies were evaluated for orbits satisfying condition (1). (Notice that pericenter of eccentric orbits can be below the marginally stable orbit of circular motion, which is at  $r = 6M$  in Schwarzschild metric.) There are three free parameters of the model,  $M, a,$  and  $e,$  which

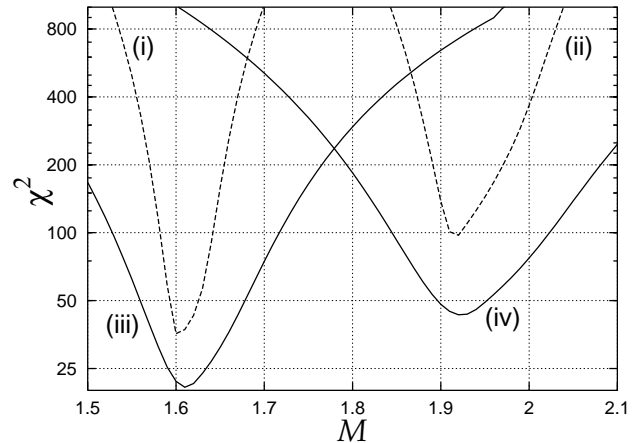


Fig. 2.— Standard  $\chi^2$  test of the best-fit mass parameter  $M$  (units of solar mass). In this figure, curves (i) and (ii) are for Sco X-1; (iii) and (iv) are for 4U 1608-52. Higher values of the mass, (ii) and (iv) ( $M = 1.92M_\odot$ ), correspond to  $\nu = \nu_\phi$ , while lower values, (i) and (iii) ( $M = 1.61M_\odot$ ), correspond to  $\nu = \nu_p$  for both sources.

can be varied to determine the best fit to the observational relation  $\Delta\nu(\nu)$ . Given these parameters, we still allow for a small variation of the integration range in  $\bar{\chi}$ , Eqs. (2)–(3), which represents uncertainty in the clumps size  $d$  of the order of 3% of  $a$ . In other words, the bounds of the interval  $\langle 0, 2\pi \rangle$  for true anomaly were varied by  $\delta\bar{\chi}(d)$  corresponding to finite-size of clumps. For this purpose one only needs to know the relation between a small variation in true anomaly and the corresponding variation in azimuthal angle:  $\delta\bar{\chi} = \xi^{1/2} [1 - k^2 \cos^2(\bar{\chi}/2)]^{1/2} \delta\phi$ , where  $k^2 = 4\mu e \xi^{-1}$  and  $\xi = 1 - 6\mu + 2\mu e$ . Near apocentre,  $\bar{\chi} \approx \pi$ , the shape of the trajectory is very close to its osculating ellipse in this point.

Figure 1 shows the range which can be covered by this model in plots of  $\Delta\nu(\nu)$  for Sco X-1 and 4U 1608-52. These sources are known to exhibit decreasing separation  $\Delta\nu$  when  $\nu$  increases (data taken from van der Klis et al. 1997, and Méndez et al. 1998). The best fit is plotted for the two interpretations of the upper-peak frequency: (i)  $\nu = \nu_\phi$  (dot-dashed line) and (ii)  $\nu = \nu_p$  (dashed), respectively. We used standard  $\chi^2$  statistics to determine the best-fit values of the parameters. The case (i) corresponds to Stella & Vietri (1999), and it yields the neutron star mass equal to  $1.92M_\odot$ , incidentally for both sources, in good agreement with their fit (apart from small difference in calculation of relevant frequencies, which translates to a 2% decrease of the best-fit mass; cf. footnote 2).  $Q$  probability is  $10^{-5}$ , defined in terms of  $\Gamma$  function and evaluated with deviations as in Fig. 1 (Press et al. 1992). The fit can be slightly improved by varying  $e$ , as suggested by Stella & Vietri, and one could also use a robust

fit. The case (ii) results in a graph of  $\Delta\nu(\nu)$  which also decreases monotonically, but the slope is flatter. We will concentrate on this case since the former one has already been examined. The best-fit mass is now significantly less,  $1.61M_{\odot}$  ( $Q = 0.4$ ). The dark shaded region in Fig. 1a corresponds to variation in  $\delta\bar{\chi}$  around the best fit. The shading covers a part of the  $(\Delta\nu, \nu_p)$  plane where the best fit is moved by such variation. Although all parameters are interconnected in the equations for frequencies, one can say that  $M$  mainly determines the absolute value of upper-peak frequency  $\nu$ , while  $a$  and  $e$  affect the sloping stripe of  $\Delta\nu(\nu)$ . Typically, in our calculations  $a$  ranges between  $6M$ – $10M$ , while  $r_p$  can plunge down to  $4M$ , determining the corresponding eccentricity  $e \lesssim 0.4$ . Keeping  $a$  fixed, the slope increases as  $e$  decreases. An almost identical area of the graph can be covered by forcing the mass to a slightly higher value,  $M = 1.70M_{\odot}$  (indicated by somewhat lighter shading in Fig. 1 for Sco X-1). In the latter case, however,  $\delta\bar{\chi}$  has to be varied in a range corresponding to somewhat larger size of the clumps, from 3 to 6 per cent of  $a$ . For 4U 1608-52, the larger scatter in the data translates to a requirement on clumps size up to  $\approx 8\%$  of  $a$ .

Let us remark that non-zero size of the spots is inevitable if they are to modulate visibly the observed radiation from the source for long periods of time. On the other hand, shearing motion destroys large spots and sets an upper limit to their sizes. If individual elements of the spots followed free Keplerian trajectories on their neighbouring orbits, the above-mentioned 3% diameter (in units of  $a$ ) would determine maximum spot size, which is still consistent with small observed widths of the peaks.<sup>4</sup> Indeed, the peaks' width increases with diameter of the sheared spots, and it should stay in agreement with the value of  $d$ , which has been determined here from scatter of data around the best fit in Fig. 1. Notice, however, that several physical mechanisms have been proposed where the spots in accretion disks could survive many orbital periods, in spite of their finite sizes. In this respect, formation of vortices was suggested by Abramowicz et al. (1992), and examined by Adams & Watkins (1995) and Bracco et al. (1999). It is speculated that these vortices durate over sufficient number of local orbital periods of the vortex center, giving rise to distinct features in observed power spectrum of the source. However, the origin of vortices is an open question so far. We thus remain on a phenomenological level of bright spots.

Figure 2 shows graphs of  $\chi^2$ , which were obtained by fitting  $a$  and  $e$ , while  $M$  was kept a fixed value within

<sup>4</sup> We thank the referee for this point. A particular example of a diminishing signal from spots which decay by shearing motion in the course of several revolutions was shown by Karas, Vokrouhlický, & Polnarev (1992).

the range 1.5–2.1 solar masses and  $\delta\bar{\chi} = 0$ . Position of the minimum of  $\chi^2(M)$  suggests the most probable mass. There are two different values of  $M$  clearly distinguished from each other, which correspond to the two cases of fitting described above, (i)  $M \approx 1.9M_{\odot}$  and (ii)  $M \approx 1.6M_{\odot}$ , although one must be cautious by interpreting such a graph when accuracy of data and the number of data points are limited. The fit can be further improved by factor  $\approx 2$  by varying  $\delta\bar{\chi}$  as described above.

Other physical processes, which have been neglected in the present text, introduce corrections to the expected range of frequencies, even if the main interpretation of relativistic orbital motion holds. Namely, one wants to estimate corrections which are caused by difference in the gravitational field of a rotating body in comparison with non-rotating Schwarzschild metric adopted here. It follows from the discussion of Morsink & Stella (1999) that no realistic equation of state for the neutron star can account for a change in kHz QPO frequencies more than 10%. An analogous conclusion holds for motion in Kerr metric with maximum rotation. It is, however, important to note that inclined orbits around a rotating body are not planar. This is due to Lense-Thirring precession which may give rise to another fundamental frequency from a tilted accretion disk (Stella & Vietri 1998; Cui, Zhang, & Chen 1998). We refer to Merloni et al. (1999) for detailed evaluation of these fundamental frequencies of spherical orbits, and for corrections to Cui et al. (1998) paper. Even in the case of non-spherical perturbations of the orbits, which should occur in realistic situations, one can introduce a *mean pericenter shift as an average* taken over many orbits, or, equivalently, over a single orbit of many individual clumps described by the probability distribution of their orbital parameters. See Karas & Vokrouhlický (1994) for such discussion of fundamental frequencies of eccentric orbits in Kerr metric. Possible appearance of averaged frequencies in the power spectrum is illustrated there too. Notice that small non-zero eccentricity of the orbits of the clumps gives rise to variations of the expected peaks' frequencies about the mean value.

## 9. Conclusion

We have verified that observed frequencies of the twin kHz QPO peaks can be reproduced by assuming modulation of the observed signal by the two fundamental frequencies of orbital motion. An alternative estimate of the neutron star mass in Sco X-1 is consistent with  $M \approx (1.6$ – $1.7)M_{\odot}$ , somewhat less than  $\approx 1.9M_{\odot}$  derived by Stella & Vietri (1999). The difference arises from interpretation of the upper peak ( $\nu_p$  vs.  $\nu_{\phi}$ ), and both possibilities still remain consistent with observational data. For orbits with negligible eccentricity we obtained identical results as those illustrated in their Fig. 1, but the present scheme obviously requires non-zero eccentricity to show up the

precession frequency in the signal. In both cases the expected range of the pair's frequency corresponds to orbital motion around a  $\lesssim 2M_{\odot}$  compact object, and their separation decreases with increasing frequency. The decrease is faster for less eccentric orbits (within the relevant range of frequencies, i.e.  $700 \text{ Hz} \lesssim \nu \lesssim 1200 \text{ Hz}$  for the upper peak). An appealing feature in the present highly simplified treatment is that the expected range, as indicated by the shading in Fig. 1, is very sensitive to the value of the central mass, and it moves away from the scale of our graphs when  $M$  is changed by  $\approx 0.3M_{\odot}$ , independently of other free parameters. Although the orbital parameters  $e$  and  $\delta\bar{\chi}$  are not strictly determined in the present treatment, it is worth mentioning that one cannot fiddle their values to obtain an increasing slope of  $\Delta\nu(\nu)$ ; this might be possible only if  $\nu \lesssim 700 \text{ Hz}$  and/or  $M \lesssim 1.5M_{\odot}$ . This argument can be used to *exclude* the present interpretation in other sources. For example, in the case of 4U 1728-34 (Méndez & van der Klis 1999) the available data do not allow a consistent fit by the above described procedure, although the peaks separation is again decreasing function of frequency.

The author acknowledges referee's suggestions regarding finite size of the blobs and critical comments on the first version of this paper. Hospitality of the International School for Advanced Studies in Trieste and support from the grants GACR 205/97/1165 and 202/99/0261 is also acknowledged.

## References

- Abramowicz, M. A., Lanza, A., Spiegel, E. A., Szuszkiewicz, E. 1992, *Nature*, 356, 41
- Adams, F. C., Watkins, R. 1995, *ApJ*, 451, 314
- Bao, G., Hadrava, P., Østgaard, E. 1994, *ApJ*, 425, 63
- Bracco, A., Provenzale, A., Spiegel, E. A., Yecko, P. 1999, in *Theory of Black Hole Accretion Disks*, eds. M. A. Abramowicz, G. Björnson, J. E. Pringle (Cambridge University Press: Cambridge)
- Chandrasekhar, S. 1983, *The Mathematical Theory of Black Holes* (Clarendon Press: Oxford)
- Cui, W., Zhang, S. N., Chen, W. 1998, *ApJ*, 492, L53
- Ford, E. C., van der Klis, M., van Paradijs, J., Méndez, M. 1998, *ApJ*, 508, L155
- Karas, V., Vokrouhlický, D. 1994, *ApJ*, 422, 218
- Karas, V., Vokrouhlický, D., Polnarev, A. 1992, *MNRAS*, 259, 569
- Kluźniak, W. 1998, *ApJ*, 509, L37
- Méndez, M. 1999, in the electronic Proceedings of the 19th Texas Symposium (Paris 1998), to appear
- Méndez, M., van der Klis, M. 1999, *ApJ*, in press
- Méndez, M., van der Klis, M., Wijnands, R., Ford, E. C., van Paradijs, J., Vaughan, B. A. 1998, *ApJ*, 505, L23
- Merloni, A., Vietri, M., Stella, L., Bini, D. 1999, *MNRAS*, 304, 155
- Miller, M. C., Lamb, F. K., Psaltis, D. 1998, *ApJ*, 508, 791
- Morsink, S., Stella, L. 1999, *ApJ*, in press
- Press W. H., Teukolsky S. A., Vetterling W. T., Flannery B. P. 1992, *Numerical Recipes* (Cambridge University Press: Cambridge)
- Stella, L., Vietri, M. 1998, *ApJ*, 492, L59
- Stella, L., Vietri, M. 1999, *Phys.Rev.Lett*, 82, 17
- van der Klis, M. 1998, in *Proceedings of the NATO ASI Ser. C*, vol. 515, *The Many Faces of Neutron Stars*, p. 337
- van der Klis, M. 1999, in *Proceedings of the Third William Fairbank Meeting on the Lense-Thirring Effect*, in press
- van der Klis, M., Wijnands, R. A. D., Horne, K., Chen, W. 1997, *ApJ*, 481, L97
- Zhang, W., Smale, A. P., Strohmayer, T. E., Swank, J. H. 1998, *ApJ*, 500, L171

# Quasi-Periodic Features due to Clumps Orbiting around a Black Hole<sup>5</sup>

Vladimír KARAS

*Astronomical Institute, Charles University Prague, V Holešovičkách 2, CZ-180 00 Praha, Czech Republic*

*E-mail: vladimir.karas@mff.cuni.cz*

The expected Fourier power-spectrum density is examined with regard to the shape and quality factor  $Q$  of features which are predicted to appear in a signal from clumps orbiting near a marginally stable orbit of a compact body. It is shown that clumps distributed randomly in a narrow range of radii produce quasi-periodic oscillations with  $Q \approx 10^2$ , similar to those observed in many low-mass X-ray binaries.

Keywords: X-rays: sources — Accretion disks — Black holes

---

<sup>5</sup>To appear in Publ. Astron. Soc. Japan (1999)

## 10. Introduction

Different types of astronomical objects exhibit periodic modulation of their signal, which contains information about the physical properties of the source. Accreting low-mass X-ray binaries (LMXBs) with quasi-periodic oscillations (QPOs) represent a particular example which has attracted much interest (for recent review see van der Klis 1999). While the origin of the QPOs is not fully understood, virtually all viable models introduce inhomogeneities (clumps of gas) in an accretion disk orbiting near to a compact neutron star or a black hole. The features which are clearly visible in the Fourier power spectra can be attributed to Doppler and lensing effects modulating the observed signal which comes from those rapidly moving clumps. Oscillations also arise due to some kind of beat frequency with neutron star spin (Miller et al. 1998). The QPO frequencies can be rather high, up to  $\approx 1300$  Hz, which is comparable with dynamical time-scale at the marginally stable orbit of a stellar-mass object,  $R_{\text{ms}}$ , suggesting distances of only several gravitational radii from the central body. Similar oscillations have been reported in X-rays from some active galactic nuclei (AGN; Papadakis, Lawrence 1995). Here, the central masses are higher by six orders of magnitude and more, so that dynamical time is a few hours. Observational data are somewhat scarce in the case of AGN, compared to Galactic sources, because the time-scales are longer and the corresponding features in the power spectrum are less sharp than in the case of LMXRBs. Still, it appears that orbiting inhomogeneities contribute to the observed X-ray variability of AGN although their presence does not explain the entire variability spectrum on a purely kinematic basis. The case of AGN is an issue of much debate, and other (magnetohydrodynamic) processes are clearly important (Abramowicz et al. 1991; Karas 1997).

We examined the expected variability power spectrum from the distribution of clumps orbiting around a compact body. In this note we employ a phenomenological description of the clumps, which has been adopted, in some form, by present models of sources with QPOs. These inhomogeneities are visible in a narrow zone of a few gravitational radii (where luminosity of the accretion disk is maximum) with the lifetime greatly exceeding the corresponding orbital periods. The above-mentioned assumption concerning the strictly localized radial distribution of the clumps is one of the distinctions of the present work from analogous studies in which the short-term featureless X-ray variability of AGN has been explored in terms of a clumpy accretion disk. Bao & Østgaard (1995) assumed a broad range of radii where the clumps exist in the disk and modulate observed signal (of the order of  $10^2$  gravitational radii), resulting in a power-law form of the Fourier power-spectrum density; in these circumstances individual peaks are smeared away. The fundamental frequency

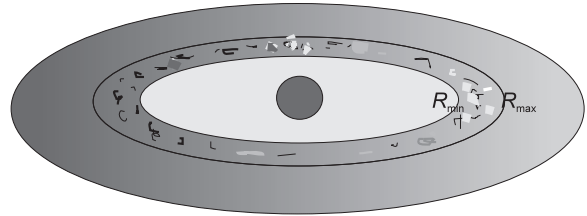


Fig. 1. In this model, clumps are distributed in a zone of several gravitational radii with their observed luminosity influenced by Doppler and lensing effects.

of orbital motion would stand out if all of the clumps were aligned along a ring with a strictly determined radius. Because this will not be the case in more realistic models, it appears relevant to ask how the width of the feature in the power spectrum is modified when the clumps are spread over a small, but non-zero, range of radius. There are at least two reasons why a localized distribution of clumps should be taken into account. First, several instability mechanisms have been proposed which could operate within distances of several  $R_g$  from the center of relativistic accretion discs and result in trapped perturbations there (Kato, Fukue 1980; Marković, Lamb 1998). Second, a non-axisymmetric structure of the disk surface could be best visible from the innermost parts of the disk where its radiation and irradiation are much stronger than farther from the center (e.g., Matt et al. 1991; Pariev, Bromley 1998). Peaks in the Fourier spectrum corresponding to the localized distribution of the clumps can be characterized by the quality factor  $Q = \nu/\Delta\nu$  (peak's centroid frequency divided by its full width at half maximum), and by harmonic content of the signal.

We considered different distributions of the clumps, as characterized by their number density and local emissivity. Here we report the main conclusion of this study, namely, we show that maximum expected values of parameter  $Q$  are of the order of one hundred and they can be as large as  $3 \times 10^2$ . We will also show typical examples of the expected power spectrum with its harmonic content which is rather strong at medium and large (i.e. edge-on) inclination.

## 11. Q-Factor and Harmonic Content of the Power Spectrum

We assumed modulation of the observed signal by self-radiating or irradiated clumps orbiting on circular orbits in the Schwarzschild metric. The superposition of independent contributions from a large number ( $N \gg 1$ ) of such clumps and the noise component are the only sources of variability in this toy model. A similar situation has been discussed in various contexts. For example, in the beat-frequency model of QPOs one considers modulation



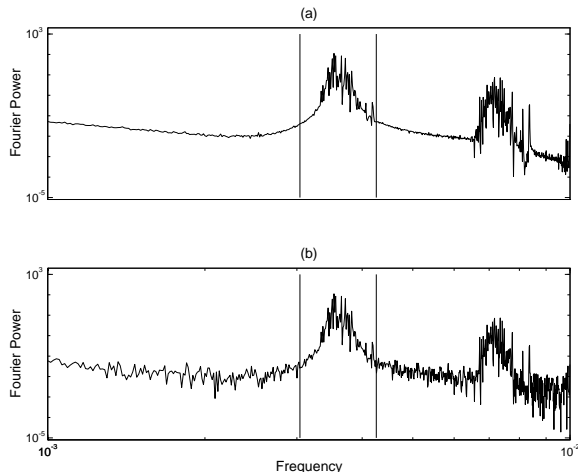


Fig. 2. Logarithmic plot of the expected power-spectrum density. The two panels correspond to: (a) pure superposition of light curves of mutually independent sources orbiting just above the marginally stable orbit; (b) an additional contribution of the high-frequency noise. Vertical bars indicate Keplerian frequencies at the edges of the clumps radial distribution, i.e. the range of fundamental frequencies  $\langle \nu_k(R_{\min}), \nu_k(R_{\max}) \rangle$ . Here, the frequency (horizontal axis) is in geometrized units, while the power spectrum (vertical axis) has an arbitrary scale. See the text for details.

of the signal by clumps near the sonic point (Miller et al. 1998). However, the assumption about circular orbits is clearly a simplification which calls for further discussion. Stella and Vietri (1999) suggest that eccentric orbits of the clumps could explain non-constant separation of twin kHz peaks detected, e.g., in Sco X-1 and 4U 1608–52. Each clump represents a spot revolving with Keplerian frequency  $\nu_k = M^{1/2} r^{-3/2} / (2\pi)$  (geometrized units). (For illustration: Keplerian frequency in Schwarzschild metric with  $M = 2M_\odot$  ranges down from its maximum value of 1.1 kHz which is acquired at  $R_{\text{ms}}$ .) All of these spots reside in a plane which coincides with an equatorial disk. The propagation of light from a source near a black hole to a distant observer has been treated by many authors within different contexts; we used one of the codes developed in the past to calculate the observed profiles of frequency integrated light curves within a geometrical-optics approximation (Karas et al. 1992; see Kato et al. 1998 for a recent text-book exposition of the subject and further references). The orbital radius  $R_s$  and the observer’s inclination  $\theta_0$  are two free parameters, which determine the

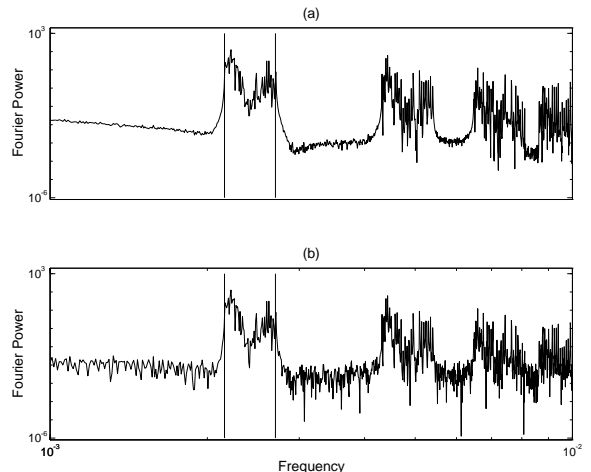


Fig. 3. As in figure 2, but for the radial distribution of sources with two maxima at slightly different radii in the disk [maximum emitted flux is superposition of two Gaussian curves, each given by equation (2)]. Two neighbouring peaks are determined by the Keplerian frequencies at radii corresponding to the local maxima in the number density of the clumps distribution.

profile produced by a single source. It turns out that the size  $d$  of the spot and its detailed shape are less important provided  $d \ll R_s$ ; this condition is assumed hereafter. Given the two parameters, numerically calculated light curves were approximated by simple formula which captures the shape of the profile (the Doppler and the lensing enhancements included). This approach enables us to carry out fast superposition of hundreds of mutually independent sources spread over a certain range of  $R_s$  (Karas 1997). To do this, one also adopts that lifetime of the sources is much longer than their orbital period; one must prescribe the radial dependence of the local emissivity (e.g., a power-law). The resulting light curve in the time domain is the sum  $F(\theta_0) = \sum_{n=1}^N F_n(R_s, \theta_0)$ , and the power spectrum,  $P(\nu)$ , is obtained by the Fourier transform  $F \rightarrow \hat{F}$  in the standard manner (Born, Wolf 1964):  $2P = \lim_{t \rightarrow \infty} [t^{-1} |\hat{F}|^2]$ .

The clumps are all placed slightly above the marginally stable orbit,  $R_{\text{ms}} = 3R_g$  (where gravitational radius in terms of the central mass is  $R_g = 2.95 \times 10^5 M/M_\odot$ ). Their distribution is characterized by the range of radii  $\Delta R$  between  $R_{\min}$  and  $R_{\max}$  ( $R_{\min} \gtrsim R_{\text{ms}}$ ; see figure 1), and by the corresponding radial dependence of the maximum flux from individual clumps,

$$F_{n,\text{max}} \propto R_s^{-\alpha_1}, \quad (1)$$

where  $\alpha_1 = \text{const}$ . We assumed locally isotropic emissivity of all sources in the frame corotating with the disk matter. The clumps are generated with random orbital phases and discarded after several orbits. The fluctuating signal is mean-subtracted and submitted to the Fourier analysis.

We also explored various modifications of the clumps distribution; particularly, the power-law (1) (with sharp edges at  $R_{\min}$  and  $R_{\max}$ ) can be substituted by a smooth Gaussian-type profile,

$$F_{n,\max} \propto \exp[-\alpha_2 (R_s - R_{\text{cen}})^2], \quad (2)$$

where  $R_{\text{cen}} = R_{\min} + \frac{1}{2}\Delta R$ ,  $\alpha_2 = \text{const} > 0$ . Such a flux distribution leads to a more familiar shape of peaks in the power spectrum, but, obviously, the choice of a particular relation requires one to specify the underlying physical mechanism producing and maintaining the clumps (which is beyond the scope of the present paper). It has been proposed and discussed by several authors that a gap in the disk can be opened where gas is swept out. This is caused by resonances due to the commensurability of the orbital period of gas with a distant disturbing secondary, or by the direct presence of a dense body (a ‘planet’) in the disk, which provokes the formation of inhomogeneities on the boundary of the gap. The resulting distribution of spots can then be approximated by superposing several profiles (2) with different  $R_{\text{cen}}$  and  $\alpha_2$ ’s.

Figure 2a shows the power-spectrum density predicted by our simulation. The graph exhibits a typical peak around the fundamental orbital frequency of the clumps,  $\nu \approx (3-4) \times 10^{-3} \text{cm}^{-1}$ , and its harmonics. This plot corresponds to eq. (2) with  $N = 250$ ,  $R_{\min} = 11M$ ,  $\Delta R = 3M$ ,  $\theta_0 = 75^\circ$ , and  $\alpha_2 = 6$ . Conversion to physical units is achieved by multiplying the frequencies in geometrized units by the factor  $2 \times 10^5 (M/M_\odot)^{-1}$ . In figure 2b, in order to account for high-frequency noise, we also superposed simulated data with a noise component characterized by zero mean and a standard deviation of  $\sigma = 5\%$ . The noise is naturally enhanced at higher frequencies, but does not greatly influence the values of  $Q$ , which refer to the peaks in the Fourier spectrum at lower frequency.

Figure 3 illustrates a more complicated situation when the radiation flux emitted by the clumps in the disk has two maxima at different radii (superposition of two profiles (2) with  $\theta_0 = 25^\circ$  and different values of  $R_{\text{cen},1} = 15M$ ,  $R_{\text{cen},2} = 17M$ ; other parameters as in figure 2). Motivation for such double-peaked radial distribution arises from possible formation of a gap in the disk. The fundamental peak in the resulting power spectrum is split into two neighbouring components, and the signal has a strong harmonic content even at moderate inclination.

Figure 4 shows the resulting quality factors for different distributions of the clumps. Here, we give the *maximum expected*  $Q$  corresponding to equation (1) with no noise component present in the signal (the values are decreased

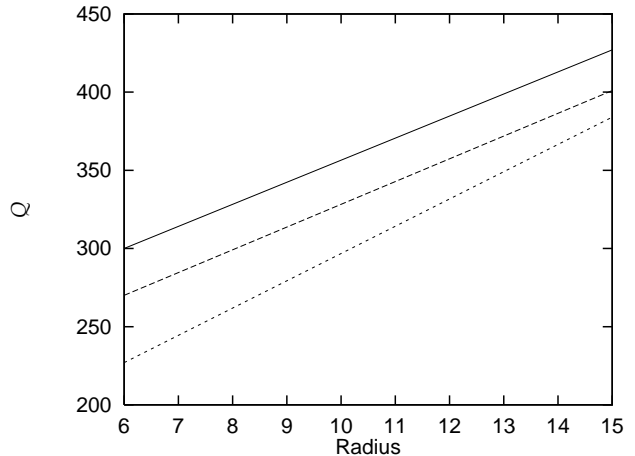


Fig. 4. Quality factor  $Q$  plotted as function of the dimensionless radius  $R_{\min}/M$  (minimum radial distance of the clumps). This plot illustrates how  $Q$  increases with  $R_{\min}$ . The values of  $Q$  are less if the clumps are distributed over wider range of radii, as characterized by  $\Delta R$ . The three lines correspond to  $\Delta R = 1M$  (solid);  $\Delta R = 2M$  (dashed);  $\Delta R = 3M$  (dotted).  $Q$  is only weakly sensitive to other parameters (see the text).

by noise, which increases the width of the peaks). Other parameters of the distribution were  $N = 250$ ,  $\alpha_1 = 1$ . Here, the values of  $Q$  were averaged over different inclinations:  $\theta_0 = 25^\circ$ ,  $50^\circ$ , and  $75^\circ$ . It turns out that  $Q$  depends only weakly on  $\theta_0$ . This conclusion can be understood by realizing that the redshift factor depends (up to relativistic corrections; Cunningham 1975) on  $\cos \theta_0$  and determines both the centroid energy of radiation from an orbiting source and the full width of the observed feature. Consequently, the  $\theta_0$ -dependence of  $Q$  is not particularly strong provided one accepts the restriction  $\theta_0 \lesssim 75^\circ$  and  $r \gtrsim R_{\text{ms}}$ , as we do in this graph. However, let us note that the harmonic content of the signal does depend on the inclination. This is because the light curve of a source orbiting at small inclination resembles a sine profile, while it becomes distorted by the lensing effect for large  $\theta_0$  ( $\gtrsim 70^\circ$ ). In other words, the power in higher harmonics increases when the inclination increases and/or the mean lifetime of the spots decreases (to be specific, we assumed 5 orbital periods as typical lifetime in our examples). The power spectrum thus has potential to reveal orientation of the disk plane. On the other hand, an excessive amount of power in the overtones can be used to restrict the validity of the model. The above-given results are not very sensitive to the assumed local size of the clumps, provided that it is much less than  $R_s$ , and to the life-time of the spots

provided it is much longer than corresponding orbital period.

In our toy model, it appears quite natural that  $Q$  increases with the radius, as can be seen in figure 4 ( $\Delta R/R_{\min}$  decreases when radius increases). One should, however, notice that  $Q \gtrsim 10^2$  also near  $R_{\text{ms}}$ . These results are not very sensitive to the values of the free parameters, and one can thus consider comparisons with observational data for particular objects (work in progress).

## 12. Conclusions

We presented a quantitative study of the expected variability power spectrum relevant for models of quasi-periodic oscillations. The orbital motion of the clumps and their distribution within a narrow range of radii are essential. The adopted phenomenological description of the source employs clumps orbiting in the Schwarzschild metric, and it can be considered to be the first approximation to more realistic models of inhomogeneous disk-type accretion flows around black holes and neutron stars. Although incompleteness of the present treatment results in free parameters which are not strictly determined here, we checked that the main results (namely, the quality parameter  $Q$ ) are not strongly sensitive to reasonable variations of parameter values.

The discussion of the power spectrum presented in this paper is a standard starting point of a Fourier analysis. It will be extended further by also examining the Fourier phases and their possible, coherence which should naturally appear due to the orbital motion of the clumps with the lifetimes substantially exceeding the dynamical time (Abramowicz et al. 1997; Karas 1997). It appears that the wavelet analysis (e.g., Starck et al. 1998) is better suited for this task than more usual approach which is offered by Fourier analysis.

The author thanks for hospitality of the International Center for Theoretical Physics in Trieste, and for support from the grants GAUK 63/98, GACR 202/98/0522, and GACR 205/97/1165 in Prague.

## References

- Abramowicz M. A., Bao G., Lanza A., Zhang X.-H. 1991, A&A 245, 454
- Abramowicz M. A., Bao G., Larsson S., Wiita P. J. 1997, ApJ 489, 819
- Bao G., Østgaard E. 1995, ApJ 443, 54
- Born M., Wolf E. 1964, Principles of Optics (Pergamon Press, Oxford), chapter 1
- Cunningham C. T. 1975, ApJ 202, 788
- Karas V. 1997, MNRAS 288, 12
- Karas V., Vokrouhlický D., Polnarev A. 1992, MNRAS 259, 569
- Kato S., Fukue J. 1980, PASJ 32, 377
- Kato S., Fukue J., Mineshige S. 1998, Black-Hole Accretion Disks (Kyoto University Press, Kyoto), chapter 3
- Marković D., Lamb F. K. 1998, ApJ 507, 316
- Matt G., Perola G. C., Piro L. 1991, A&A 247, 25
- Miller M. C., Lamb F. K., Psaltis D. 1998, ApJ 508, 791
- Papadakis I. E., Lawrence A. 1995, MNRAS 272, 161
- Pariev V. I., Bromley B. C. 1998, ApJ 508, 590
- Stella L., Vietri M. 1999, Phys. Rev. Lett. 82, 17
- Starck J.-L., Murtagh F., Bijaoui A. 1998, Image Processing and Data Analysis (Cambridge University Press, Cambridge), chapter 1
- van der Klis M. 1999, in Proceedings of the Third William Fairbank Meeting, in press; astro-ph/9812395